SLAC–PUB–8666
October 2000

Planar Dielectric Accelerator Structures at W-band*

Marc E. Hill, Richard S. Callin, Xintian E. Lin and David H. Whittum
Stanford Linear Accelerator Center, Stanford University, Stanford, CA 94309

Abstract

We describe the operating priciples, design, fabrication, assembly, and bench-test of a miniature planar dielectric traveling-wave accelerator structure made from dielectric brazed to oxygen-free electronic grade (OFE) copper. This work focusses on alumina ceramic (AL995) and diamond as dielectrics. This two-port device is matched to WR10 at input and output, and designed for charged particle acceleration at 91.392 GHz (W-band).

Submitted to Review of Scientific Instruments

*Work supported by Department of Energy contract DE–AC03–76SF00515.

Planar Dielectric Accelerator Structures at W-band

Marc E. Hill, Richard S. Callin, Xintian E. Lin, and David H. Whittum

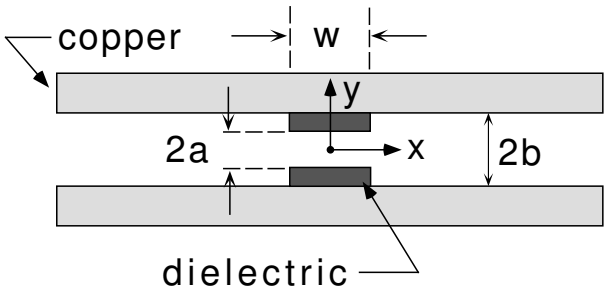

Fig. 1. A cross-section of the planar dielectric accelerator. The particle beam travels in the z direction, out of the page.

Abstract— **We describe the operating priciples, design, fabrication, assembly, and bench-test of a miniature planar dielectric traveling-wave accelerator structure made from dielectric brazed to oxygen-free electronic grade (OFE) copper. This work focusses on alumina ceramic (AL995) and diamond as dielectrics. This two-port device is matched to WR10 at input and output, and designed for charged particle acceleration at 91.392 GHz (W-band).**

I. Introduction

High energy physics requires a high-energy accelerator, and a compact machine for this purpose requires high electric field gradient. Breakdown, trapping and pulsed heating dictate that such a high field requires a high-frequency structure, and we are presently pursuing the design, fabrication and test of components needed for a charged particle accelerator at W-band. In previous work we have reported development and test of vacuum and high-power compatible flanged waveguide (WR10), alumina ceramic windows [1], squeeze-type phase-shifters [2], and a single cell accelerator structure [3]. In this work we describe for the first time the design, fabrication, and bench-test of a W-band accelerator, based on a traveling-wave planar dielectric structure.

Previous attempts have been made to fashion reliable and robust multi-cell traveling-wave structures at mm-wave frequencies [4]; however these have proved difficult to assemble accurately, prone to failure of thin coupling irises, and difficult to bond at current-carrying joints [5]. In the meantime we have chosen to pursue an alternate approach to fashion a structure amenable to high-gradient acceleration employing dielectric loaded waveguide in a slab geometry.

The structure itself consists of two smooth dielectric slabs forming a transmission line as seen in Fig. 1. The dimensions are chosen to provide a phase velocity equal to the speed of light and thus synchronism with a relativistic particle beam. The ends of the transmission line are coupled to WR10 waveguide through coupling cavities designed to match to a traveling wave at 91.392 GHz. A great virtue of such a longitudinally invariant structure is that small features such as disks are eliminated. At the same time the tunability afforded by the adjustable gap ($2a$ in Fig. 1) relaxes machining tolerances significantly. In addition, the field configuration is such that the surface electric field at the copper is smaller than the on-axis field. In contrast, disk loaded waveguide typically has a surface field *twice* the accelerating gradient. Another virtue is that the side opening affords high vacuum conductance and wakefield damping.

In this paper we describe the design considerations, fabrication and bench-test of such a "composite" accelerator – one consisting of copper and dielectric. Our criteria for choice of dielectric were vacuum compatibility, breakdown threshold, moderate permittivity ($\varepsilon_r < 10$) for reasonable group velocity (giving reasonable maching tolerances), and low loss-tangent. We pursued the use of two materials: alumina ceramic and carbon vapor deposition (CVD) diamond, with relative permittivities at W-band of 9.5 and 5.5, respectively. Diamond is of great interest [6] for high-gradient work, where heating and breakdown are concerns.

II. Principle of the Slab Accelerator

A smooth conducting waveguide cannot provide acceleration due to phase velocity in excess of the speed of light. Addition of a dielectric liner can however slow down the wave and permit synchronous interaction with a charged particle beam to provide acceleration. The earliest – and ongoing – studies of such structures concentrated on a cylindrical geometry operating at X-band [7]. At W-band (8× smaller), a cylindrical geometry is difficult to fabricate, and it is for this reason that we have pursued the slab geometry of Fig. 1.

To illustrate the principles of the planar dielectric accelerator, let us examine the fields in a parallel plate configuration. The plates are lined with dielectric material of relative permittivity ε_r, separated with a vacuum gap of distance $2a$, as seen in Fig. 1. For illustration we analyze the fields in the limit $w/b \gg 1$. The solution of the Helmholtz equation for the axial electric field is even in y and for $y > 0$ given by the real part of

$$E_z = G e^{ik_z z - i\omega t} \begin{cases} \cos(k_1 y) & y < a \\ \dfrac{\cos(k_1 a)}{\sin[k_2(a-b)]} \sin[k_2(y-b)] & a < y < b \end{cases} \quad (1)$$

Work supported by the U.S. Department of Energy under contract DE-AC03-76SF00515.

M.E. Hill is with the Department of Physics at Harvard University, Cambridge, MA 02138.

R.S. Callin, X.E. Lin and D.H. Whittum are with the Stanford Linear Accelerator Center, Stanford University, Stanford, California 94309.

where G is the on-axis gradient, k_z is the longitudinal wave number, ω is the angular frequency, and k_1 and k_2 are the transverse wave numbers in the vacuum and dielectric respectively, and satisfy

$$k_1^2 = \frac{\omega^2}{c^2} - k_z^2, \tag{2}$$

$$k_2^2 = \varepsilon_r \frac{\omega^2}{c^2} - k_z^2. \tag{3}$$

The dispersion relation is

$$\tan(k_1 a)\tan(k_2[b-a]) = \varepsilon_r \frac{k_1}{k_2}. \tag{4}$$

For acceleration we also have the requirement that the wave be synchronous with a speed of light particle $\omega/k_z = c$. This implies

$$k_1 = 0 \tag{5}$$

$$k_2 = \frac{\omega}{c}\sqrt{\varepsilon_r - 1}. \tag{6}$$

The field components corresponding to $k_1 = 0$ are

$$E_z = G e^{ik_z z - i\omega t} \begin{cases} 1 \\ \dfrac{\sin(k_2[y-b])}{\sin(k_2[a-b])} \end{cases} \tag{7}$$

$$E_y = ik_z G e^{ik_z z - i\omega t} \begin{cases} -y \\ \dfrac{1}{k_2}\dfrac{\cos(k_2[y-b])}{\sin(k_2[a-b])} \end{cases} \tag{8}$$

$$B_x = -\frac{ik_z}{c} G e^{ik_z z - i\omega t} \begin{cases} -y \\ \dfrac{\varepsilon_r}{k_2}\dfrac{\cos(k_2[y-b])}{\sin(k_2[a-b])} \end{cases} \tag{9}$$

From this analysis a number of practical formulas emerge. One may show that the ratio of surface field to accelerating field is

$$\frac{E_y}{G} = \sqrt{\left(\frac{\omega a}{\varepsilon_r c}\right)^2 + \frac{1}{\varepsilon_r - 1}} \tag{10}$$

which is a fraction smaller than 1 for our examples. The power flowing through the structure is

$$P = \frac{\omega^2}{c^2}\frac{G^2}{Z_0} W \left[\frac{2a^3}{3} + \frac{b-a}{a}\left(\frac{a^3}{\varepsilon_r} + \frac{\varepsilon_r a}{k_2^2}\right) + \frac{a}{k_2^2}\right] \tag{11}$$

where W is the width of the structure. The group velocity at synchronism is

$$\frac{v_g}{c} = \frac{1 + A/\varepsilon_r}{1 + A}, \tag{12}$$

where we abreviate

$$A = \left(\frac{b}{a} - 1\right)\left[1 + \frac{\varepsilon_r}{k_2^2 a(b-a)} + \left(\frac{\varepsilon_r}{k_2 a}\right)^2\right] \tag{13}$$

A useful approximate solution to the dispersion relation corresponds to the limit $\varepsilon_r \left(\frac{b-a}{a}\right) \gg 1$ and is given by

$$k_2 \approx \frac{\pi/2}{b-a}. \tag{14}$$

An illustrative design would take $G = 1$ GV/m, in a structure with resonance at $\omega/2\pi \approx 91.4$ GHz, dimensions $a = 300$ μm, $b = 550$ μm, and $\varepsilon_r = 9.5$. The group velocity is given by $v_g/c \approx 1/\varepsilon_r \approx 0.1$ and taking $W \approx b$ the power required is 500 MW. This structure scaled down from a free-space wavelength of 3.3 mm to 1.5 μm would require 100 W for the same gradient.

III. Design and Tolerances

In general, design of an accelerator structure proceeds from an optimization of

$$\left[\frac{R}{Q}\right] = \frac{G^2 v_g}{\omega P} \tag{15}$$

and while the example of Sec. II is useful as a guide, it is possible to be more precise with the help of a finite difference electromagnetics code *GdfidL* [8]. For illustration, we present two structure designs each using alumina ceramic and diamond. Dimensions were chosen compromising between high $[R/Q]$ and adequate beam aperture with synchronism at the design frequency held constant. With the aid of *GdfidL*, we arrived at the geometrical parameters for the structures listed in Table I. This table summarizes design parameters for an alumina structure (column 1); its slab counterpart (column 2) is obtained holding b/a constant. Similarly, diamond and its slab counterpart are listed in columns 3 and 4.

An infinite length structure is modelled numerically by one with finite length having periodic boundary conditions. The numerically computed Q resulting from sidewall copper and dielectric loss in this finite length structure may then be employed to determine the attenuation length in the traveling wave structure by the relation

$$\alpha = \frac{\omega}{2Qv_g}. \tag{16}$$

The field-solver also provides the dispersion characteristics of the various structure modes. For illustration, dispersion curves for the monopole modes of the diamond structure (column 3, Table I) are illustrated in Fig. 2. The accelerating mode corresponds to the curve labelled HEM_{11} in

TABLE I

List of geometrical parameters for example structures, with resonance at 91.4 GHz.

	GdfidL	Slab	*GdfidL*	Slab
ε_r	9.5	9.5	5.5	5.5
a (μm)	360	300	272	230
b (μm)	650	550	680	575
W (μm)	800	—	1360	—
v_g/c	0.1	0.1	0.2	0.2
$[R/Q]$ $\left(\frac{k\Omega}{m}\right)$	90	—	94	—
α (m^{-1})	6.4	6.8	2.2	3.0
Q	1500	1400	2200	1600
E_y/G	0.6	0.6	0.7	0.5

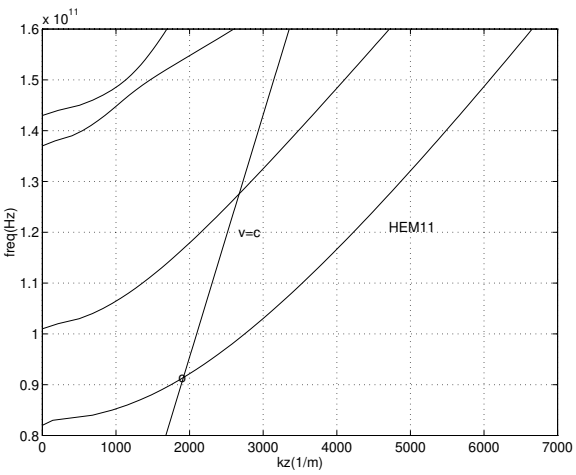

Fig. 2. The dispersion diagram for the lowest monopole modes and the speed of light line $v = c$ for a diamond structure, for illustration.

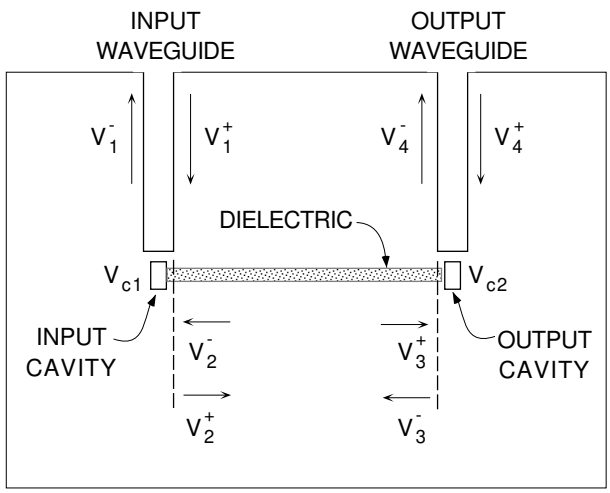

Fig. 3. Sketch of dielectric structure indicating input, output, and transmission line voltages.

Fig. 2, and the operating frequency is indicated by a circle. The wave number at the operating frequency is $k_z = \omega_0/c$.

As in a conventional structure, synchronism imposes tolerances on the geometry. The sensitivities to dielectric thickness ($d = b - a$), width (w), and gap distance ($2a$) are listed in Table II for two sample structures. Conversely the coefficients of Table II permit correction of uniform errors of the geometry by adjustment of the gap distance ($2a$), albeit with some compromise in $[R/Q]$ or beam aperture.

Such tuning errors cause a deviation of phase velocity from c that results in particle phase slippage from the RF phase. A *uniform* deviation of Δk_z from the speed of light line will result in a linear phase slip

$$\delta\phi(z) = \Delta k_z z. \tag{17}$$

The result is a reduction in the voltage gain experienced by a particle traversing the structure,

$$\frac{V}{V_0} = \frac{1}{l}\left|\int_{-l/2}^{l/2} e^{j\delta\phi(z)}dz\right| = \mathrm{sinc}\left(\frac{\Delta k_z l}{2}\right), \tag{18}$$

TABLE II

Phase sensitivity to dielectric thickness (d), width (w), and gap distance (a) for the structures described in Table I. Units are $\mathrm{m}^{-1}/\mu\mathrm{m}$.

	Alumina	Diamond
$\frac{\delta k_z}{\delta d}$	34	15
$\frac{\delta k_z}{\delta w}$	3.2	1.3
$\frac{\delta k_z}{\delta a}$	2.9	2.5

where V_0 is the voltage gain absent errors. It follows that allowance of 10% voltage reduction in a structure with $l \approx 2.54$ cm requires $|\Delta k_z/k_z| < 3\%$. Presently, we show that we were able to tune the structure well within this limit.

Another kind of error of potential concern, corresponds to a *linear taper* in w or d. This kind of error cannot be tuned away, in contrast to the previous *uniform* error. Considering $w = w_0 + \theta_w z$ where θ_w is the taper angle, the phase velocity corresponds to axial wavenumber

$$k_z(z) = k_z(0) + \frac{\delta k_z}{\delta w}\theta_w z. \tag{19}$$

The phase slip $\delta\phi$ is found by integrating the phase velocity along the length

$$\delta\phi(z) = \frac{1}{2}\frac{\delta k_z}{\delta w}\theta_w z^2. \tag{20}$$

A calculation like that of Eq. (18) gives

$$\frac{V}{V_0} = \frac{|C(\zeta) + iS(\zeta)|}{\zeta}, \tag{21}$$

$$\zeta = \frac{l}{2}\sqrt{\frac{\theta_w}{\pi}\frac{\delta k_z}{\delta w}} \tag{22}$$

where C and S are the Fresnel functions. For a 10% voltage reduction and $l \approx 2.54$ cm, the thickness (d) variation must be held to 13 μm from one end to the other. The width (w) taper must be less than 72 μm. These numbers represent at least a factor of 3 improvement (increase) in the tolerance over that for a conventional disk loaded structures.

IV. Circuit Model

In the foregoing we have discussed the traveling wave structure of Fig. 1; however, this is only part of the millimeter wave circuit. The complete structure forms the circuit indicated in Fig. 3, consisting of connecting waveguide, an input coupling cavity, the dielectric transmission line, an output coupling cavity, and another connecting

waveguide. As an accelerator, and an rf circuit, this system may be modelled as two coupled cavities connected by a transmission line. The transmission line model parameters are L, the length of the dielectric line, k_z, the axial wavenumber, and α, the attenuation constant.

The input cavity is characterized by the parameters: Q_{e_1}, the external quality factor quantifying the coupling between the cavity and waveguide, Q_{e_2}, characterizing coupling between cavity and dielectric line, ω_1, the cavity resonance frequency, and Q_{w_1}, the cavity wall Q. In the time-domain, the two-port cavity model takes the form

$$\left(\frac{d^2}{dt^2}+\frac{\omega_1}{Q_{L_1}}\frac{d}{dt}+\omega_1^2\right)V_{c_1}=2\frac{\omega_1}{Q_{e_1}}\frac{d}{dt}V_1^+ + 2\frac{\omega_1}{Q_{e_2}}\frac{d}{dt}V_2^+ \tag{23}$$

to give the steady-state result at angular frequency ω,

$$V_{c_1}=2Q_{L_1}e^{-i\psi_1}\cos\psi_1\left(\frac{V_1^+}{Q_{e_1}}+\frac{V_2^+}{Q_{e_2}}\right) \tag{24}$$

where $1/Q_{L_1}=1/Q_{e_1}+1/Q_{e_2}+1/Q_{w_1}$ and

$$\tan\psi_1=Q_{L_1}\left(\frac{\omega_1}{\omega}-\frac{\omega}{\omega_1}\right) \tag{25}$$

From Eq. (24) we get the scattering matrix elements for the input cavity viewed as a two-port cavity

$$A_{11}=\frac{V_1^-}{V_1^+}=\frac{V_{c_1}-V_1^+}{V_1^+}=2\frac{Q_{L_1}}{Q_{e_1}}e^{-i\psi_1}\cos\psi_1-1 \tag{26}$$

$$A_{12}=A_{21}=n\frac{V_{c_1}-V_2^+}{V_1^+}=\frac{2Q_{L_1}e^{-i\psi_1}\cos\psi_1}{\sqrt{Q_{e_1}Q_{e_2}}} \tag{27}$$

$$A_{22}=\frac{V_2^-}{V_2^+}=\frac{V_{c_1}-V_2^+}{V_2^+}=2\frac{Q_{L_1}}{Q_{e_2}}e^{-i\psi_1}\cos\psi_1-1 \tag{28}$$

where $n_1=\sqrt{Q_{e_1}/Q_{e_2}}$. In the same way we arrive at the scattering matrix elements for the output cavity

$$B_{11}=\frac{V_3^-}{V_3^+}=\frac{V_{c_2}-V_3^+}{V_3^+}=2\frac{Q_{L_2}}{Q_{e_3}}e^{-i\psi_2}\cos\psi_2-1 \tag{29}$$

$$B_{12}=B_{21}=n_2\frac{V_{c_2}-V_4^+}{V_3^+}=\frac{2Q_{L_2}e^{-i\psi_2}\cos\psi_2}{\sqrt{Q_{e_3}Q_{e_4}}} \tag{30}$$

$$B_{22}=\frac{V_4^-}{V_4^+}=\frac{V_{c_2}-V_4^+}{V_4^+}=2\frac{Q_{L_2}}{Q_{e_4}}e^{-i\psi_2}\cos\psi_2-1 \tag{31}$$

where $n_2=\sqrt{Q_{e_3}/Q_{e_4}}$. Concatenating the input cavity S-matrix, the S-matrix for the transmission line, and the output cavity we arrive at the S-matrix for the system as a whole as in Fig. 3,

$$S=\begin{pmatrix} A_{11}+\frac{\Gamma^2A_{12}B_{11}A_{21}}{1-\Gamma^2B_{11}A_{22}} & \frac{\Gamma A_{12}B_{12}}{1-\Gamma^2B_{11}A_{22}} \\ \frac{\Gamma B_{21}A_{21}}{1-\Gamma^2B_{11}A_{22}} & B_{22}+\frac{\Gamma^2B_{21}A_{22}B_{12}}{1-\Gamma^2B_{11}A_{22}} \end{pmatrix} \tag{32}$$

The transmission line coupling the two cavities has phase length and attenuation described by $\Gamma=e^{-(ik_z+\alpha)L}$, where the dispersion relation for the transmission line is determined by simulation. Referring to Fig. 3, S provides direct comparision with bench tests via

$$\begin{pmatrix} V_1^- \\ V_4^+ \end{pmatrix}=S\begin{pmatrix} V_1^+ \\ V_4^- \end{pmatrix}. \tag{33}$$

We employ Eq. (32) for comparison with measurements, as we describe below.

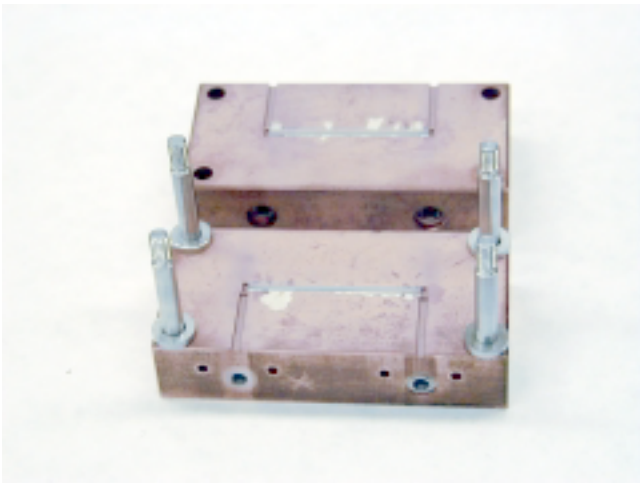

Fig. 4. Picture of a planar dieletric accelerator structure made from two identical halves. The alumina strip is brazed to the center and located between the input and output waveguide and coupling cavities.

V. Fabrication and Cold-Test

The first step of the fabrication process was to machine the dielectric. The alumina was ground to its final dimension; the diamond was laser cut. The results were essentially 1" long "toothpicks" with cross-sections of 0.3×0.8 mm^2 for the alumina and 1.3×0.4 mm^2 for the diamond with tolerences in the range 5-10 μm.

The dielectric strips were aligned to the center of the flats using a precision machined fixture, and brazed to the copper substrate using an active braze alloy (ABA) from WesCo, CuSilABA (78% Cu, 20%Ag, 2%Ti). Happily, we have not yet seen dielectric cracking or copper warping due to stresses induced by the braze process. In priciple, this is a concern given differential expansion at the 810°C braze temperature of the copper and alumina (diamond) with the expansion coefficients of 2×10^{-5} and 1×10^{-6} (0.8×10^{-6}).

After the dielectric was brazed, we cut the input and output waveguides and coupler cavities using stub electro-discharge machining (EDM). Location of the cavity and dielectric centers were required to be within 5 μm. After a first cut of the cavities, photo seen in Fig. 4, we assessed the state of the structure employing a W-band vector network analyzer (VNA) [9]. In this way we could determine the transmission and reflection characteristics, and make comparison with Eq. (32), employing the external Q's, wall Q's, and the resonance frequencies.

Finding that wall quality factors were rather low in previous EDM cavity studies, we performed a stub EDM test-

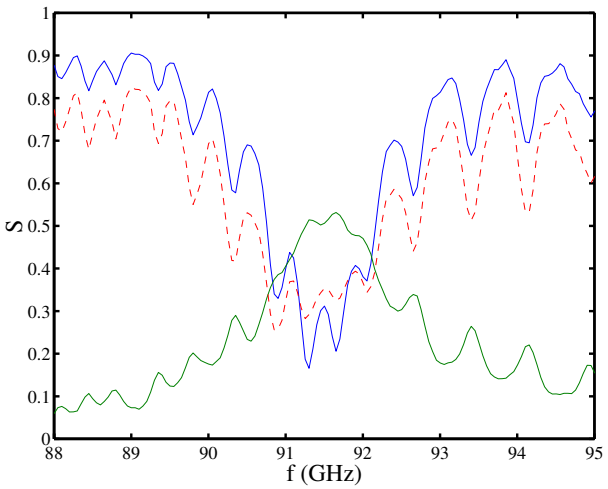

Fig. 5. S-matrix parameters as measured with the VNA including the power sum $S^2 = S_{11}^2 + S_{12}^2$ (dashed).

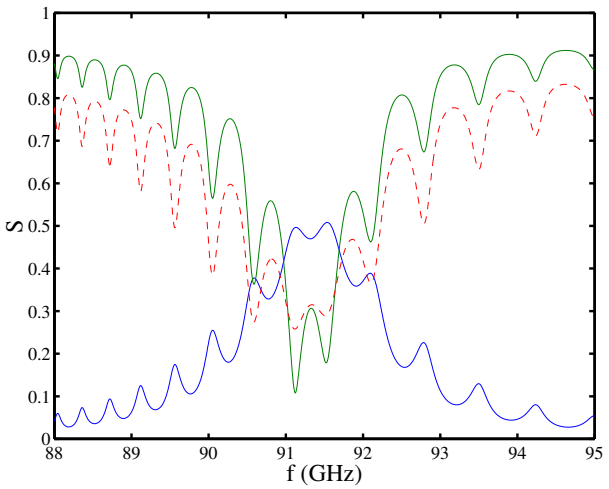

Fig. 6. S parameters from Eq. (32) for a planar dielectric accelerator structure with realistic dielectric waveguide characteristics including dispersion and attenuation. $S^2 = S_{11}^2 + S_{12}^2$ (dashed)

cut of additional stand-alone coupling cavities to measure the quality of the cut structures. We found that the wall Q of the cavity could be improved by "sand blasting" the cavity with 10 μm alumina ceramic powder. We saw a 20% improvement in wall Q and no appreciable change in external Q or resonance frequency.

In this way, after three iterations of cutting and measurement, we had cut the coupler cavities to proper frequency and coupling, and arrived at a circuit characterized by the scattering matrix parameters depicted in Fig. 5 for the alumina example.

Using the circuit model already discussed and comparing with the data of Fig. 5 with the modelled results shown in Fig. 6, we inferred the circuit parameters listed in Table III. Independent measurement of the "sand-blasted" coupling cavities confirmed Q_{w_1} and Q_{e_1}.

VI. Bead Pull

As discussed earlier, the phase velocity of the structure must be maintained to within ±3%. The phase velocity was measured by means of a non-resonant bead pull. The field perturbation was provided by a 100 μm diameter stainless steel hypodermic needle stretched transversely across the structure. The perturbation caused by this needle in a non-resonant structure takes the general form [10],

$$\Delta S_{11} = \frac{i\omega}{2P}\left(\epsilon\alpha_e E^2 - \mu\alpha_m H^2\right) e^{-2\gamma z} \qquad (34)$$

TABLE III

Circuit model parameters describing the accelerator as a series of lumped elements for the alumina example with $L = 2.54$ cm.

$\omega_1/2\pi$	Q_{w_1}	Q_{e_1}	Q_{e_2}
91.4 GHz	1000	80	130

$\omega_2/2\pi$	Q_{w_2}	Q_{e_3}	Q_{e_4}	α
91.5 GHz	130	80	1000	14 m^{-1}

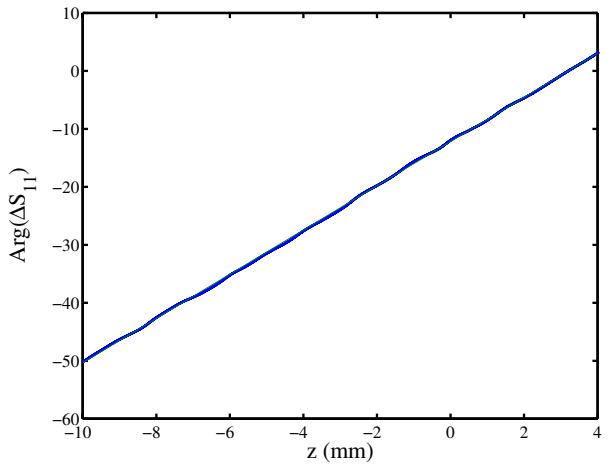

Fig. 7. Phase of ΔS_{11} as measured from bead pull overlaid with the theoretical result, confirming $k_z = \omega/c$.

where $\gamma = (ik_z + \alpha)$, P is the power and the polarizabilities of the needle are described by α_e and α_m. In fact, inference of the complex wave number is independent of α_e and α_m. The wavenumber, k_z, may be inferred from the phase of ΔS_{11}, shown in Fig. 7, for the alumina example. This structure was tuned by adjusting the gap distance ($2a$) to yield a phase velocity within 0.1% of the speed of light.

The attenuation length of the ceramic may be inferred from the amplitude of ΔS_{11} shown in Fig. 8, well fit by $1/\alpha = 73$ mm. These data may be compared with those listed in Table I. While we cannot distinguish dielectric and copper loss by our measurements, our experience with copper waveguide of similar manufacture corresponds to an effective surface resistance 30% over that of an ideal smooth OFE copper surface. From this and our observed figure for attentuation, we may infer a loss-tangent of 1×10^{-3} for alumina, lying in the range of reported values $0.8 - 1.6 \times 10^{-3}$ at W-Band.

In parallel with the alumina structure, we have performed a similar study of a diamond dielectric structure

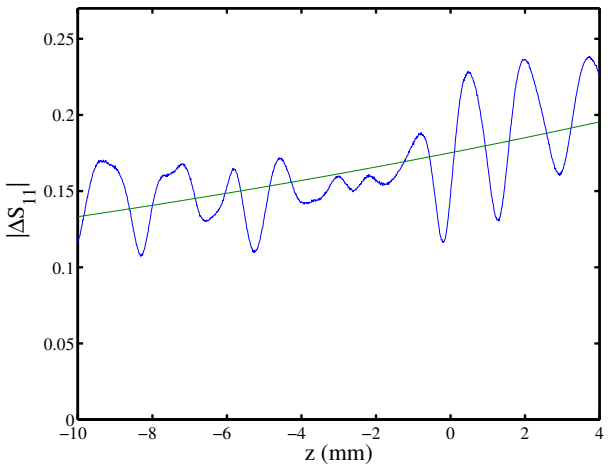

Fig. 8. Attenuation length as measured from a bead pull, overlaid with the least-squares fit with decay length, $1/\alpha = 73$ mm.

including design, fabrication and bench-test. The data for our diamond structure revealed that our diamond samples were of low quality, with a dielectric constant of 5.7 rather than 5.5 and a high loss tangent in the 10^{-2} range.

VII. Discussion

We have presented for the first time an assembled and bench-tested W-Band dielectric accelerator. For some years discussion of mm-wave accelerator structures has centered on the difficulty of fabrication of miniature disk-loaded guide [11], [12]. Here we have seen that an alternative approach employing a smooth dielectric loaded guide is quite feasible. Clearly, assembly, cleaning, and fine-tuning on the bench are critical in arriving at accurately tuned input and output cavities, and high wall Q's. As for lower frequency accelerator work, fabrication goes hand-in-hand with rf measurements on the bench.

This structure was subsequently installed on an electron beamline [13] and excited by a 0.5 A, 100 ns relativistic beam developing a circulating power of 200 kW, corresponding to a peak on-axis gradient of 20 MV/m. No indication of ceramic charging, breakdown, or dielectric damage was observed and good vacuum integrity was maintained (10^{-8} torr in the beamline). Further details of the tests with beam are the subject of a future work.

VIII. Ackowledgements

The authors thank O. Millican and D. Shelly for their expert assistance in manufacture of the structures.

References

[1] M. E. Hill, R. S. Callin and D. H. Whittum, "High-power vacuum window in WR10," *IEEE Trans. MTT*, to be published.

[2] M. E. Hill, R. S. Callin, M. Seidel and D. H. Whittum, "High power squeeze type phase shifter at W-band," sub. to *IEEE Trans. MTT*.

[3] M. E. Hill, W. R. Fowkes, X. E. Lin and D. H. Whittum, "Beam-cavity interaction circuit at W-band," *IEEE Trans. MTT*, to be published.

[4] P.J. Chou, G.B. Bowden, M.R. Copeland, A. Farvid, R.E. Kirby, A. Menegat, C. Pearson, L. Shere, R.H. Siemann, J.E. Spencer, and D.H. Whittum, *Advanced Accelerator Concepts*, AIP Conf. Proc. 398 (AIP, New York, 1997) pp. 501-517.

[5] N.M. Kroll, D. C. Vier, M.E. Hill, X.E. Lin, R.H. Siemann, D.H. Whittum, and D.T. Palmer, "Planar accelerator structures for millimeter wavelengths," *Proceedings of the 1999 Particle Accelerator Conference* (IEEE, New York, 1999) 3612-3614.

[6] X.E. Lin, "Diamond coating in accelerator structures," *Advanced Accelerator Concepts*, W. Lawson, C. Bellamy, and D.F. Brosius, eds., AIP Conf. Proc. 472 (AIP, New York, 1999) pp. 676-685.

[7] P. Zou, W. Gai, R. Konecny and T. Wong, "Construction and testing of an 11.4-GHz dielectric structure based traveling wave accelerator," *Proceedings of the 1999 Particle Accelerator Conference* (IEEE, New York, 1999) pp. 3618-3620

[8] W. Bruns, "GdfidL: A finite difference program for arbitrarily small perturbations in rectangular geometries", *IEEE Trans. Magn.* **32**, pp. 1453-1456, 1996.

[9] R.H.Siemann, "W-Band vector network analyzer based on an audio lock-in amplifier", SLAC-PUB-7884.

[10] C.W. Steele, "A non-resonant perturbation theory," *IEEE Trans. Magn.* **14** (1966) pp. 70-74

[11] H. Henke, "Planar mm-Wave RF Structures," *Proceedings 7th Workshop on Advanced Accelerator Concepts* (AIP conference proceedings; 398) Edited by S. Chattopadhyay, J. McCullough, P. Dahl. (AIP, Woodbury, 1997) pp. 485-500.

[12] W. Schnell, "High Frequency Linear Colliders," *Proceedings 4th European Particle Accelerator Conference* (EPAC 94) Edited by V. Suller and Ch. Petit-Jean-Genaz (World Scientific, River Edge, 1994) pp. 368-372

[13] R. D. Ruth *et al.*, "Results from the SLAC NLC test accelerator," *Proceedings: 1997 IEEE Particle Accelerator Conference*, Edited by M. Comyn, M.K. Craddock, M. Reiser, J. Thomson (Piscataway, IEEE, 1998) pp. 439-443